Experimental validation of genetic programming for heat exchanger circuitry optimization

Applied Thermal Engineering 288 (2026) 129517

Contents lists available at ScienceDirect

Applied Thermal Engineering

journal homepage: www.elsevier.com/locate/apthermeng

Research Paper

Experimental validation of genetic programming for heat exchanger circuitry optimization

N. Giannetti [a,*], C.H. Kim [a], F. Della Santa [b,c], Y. Sei [d], K. Enoki [e], K. Saito [f]

[a] Sustainable Energy & Environmental Society Open Innovation Research Organization, Institute for Energy and Environmental system, Waseda University, Tokyo 169-8050, Japan
[b] Department of Mathematical Sciences, Politecnico di Torino, Turin 10129, Italy
[c] Gruppo Nazionale per il Calcolo Scientifico IndaM, Rome 00185, Italy
[d] Department of Informatics, The University of Electro-Communications, Tokyo 182-8585, Japan
[e] Department of Mechanical and Intelligent Systems Engineering, The University of Electro-Communications, Tokyo 182-8585, Japan
[f] Department of Applied Mechanics and Aerospace Engineering, Waseda University, Tokyo 169-8555, Japan

ARTICLE INFO

Keywords:
Circuitry optimization
Genetic programming
Heat exchanger
Experimental validation

ABSTRACT

Although evolutionary circuitry optimization has been recognized as a cost-effective method in recent research, it remains to be experimentally verified. Accordingly, this study reports on experiments conducted to validate the effectiveness of genetic programming for heat exchanger circuitry optimization. The numerical optimization results of the evaporator are identified for R32 in a capacity range between 3 and 4 kW and for the given airside features, thereby suggesting optimal branching and patterning characteristics obtained by implementing genetic operators through genetic programming for 3.0, 3.5, and 4.0 kW design conditions. Airside design, including fin package, remains unchanged across all investigated capacities. The manufacturability of the optimized solutions is enhanced by introducing additional constraints. Consequently, baseline and optimized heat exchangers are manufactured and tested using dedicated equipment. The test results validate the numerical model, with 66.7 % of the temperature deviation within ±1.0 K and pressure deviations within ±5.0 % of the measured values, as well as verify the benefits achievable through optimized branching and patterning. The optimized configurations at 3- and 4-kW capacity achieve inlet saturation temperatures that are 2.7 K and 4.1 K higher, respectively. The circuitry optimized at 3 kW results in an 18.0 kPa increase in pressure drop, whereas the optimization conducted at 4 kW produces an 83.5 kPa decrease. These effects translate into corresponding improvements of 18.9 % and 12.8 % in the measured coefficient of performance. The results support the development of more accurate simulations and pave the way for the practical implementation of genetic programming for actual product development.

1. Heat exchanger circuitry optimization

Research and development aimed at introducing low global warming potential (GWP) refrigerants into refrigeration and air-conditioning equipment to prevent global warming are entering full swing. However, when introducing next-generation refrigerants, evaluating not only their safety and GWP but also the global warming impact caused by CO_2 emissions from energy consumption is essential. Therefore, the actual operating performance of the equipment is one of the most critical factors. However, at present, refrigerants are selected without sufficient evaluation of the equipment performance.

The search for optimal refrigerant circuitry features is a cost-effective optimization procedure for maximizing the performance of heating and cooling systems [1–5] and minimizing their environmental impact for a given refrigerant. Significant effort has been devoted to mitigating inefficiencies arising from airflow nonuniformities through tailored circuitry designs [5]. Proposed compensation strategies include modifying feeder tube configurations [6], implementing individual valve control [7], adopting interleaved circuitry arrangements [8], and adjusting the number and length of subcircuits [9].

Heat exchangers are composed of multiple tubes that can be combined into multiple possible refrigerant flow paths, especially considering the arbitrary numbers and locations of the splitting and merging junctions. Consequently, the correspondingly large search space cannot

* Corresponding author.
E-mail address: giannetti.n@aoni.waseda.jp (N. Giannetti).

https://doi.org/10.1016/j.applthermaleng.2025.129517
Received 16 September 2025; Received in revised form 11 December 2025; Accepted 16 December 2025
Available online 17 December 2025

generally be managed with trial and error or empirical procedures, and theoretical approaches are limited to oversimplified models. For instance, [10,11] developed simplified analytical approaches that consider constant transport properties but do not provide answers for defining the numbers and locations of splitting and merging within the refrigerant circuitry.

Evolutionary algorithms are optimization methods inspired by biological evolution that provide a more effective convergence ability over extensive search spaces, meeting the possibility of taking advantage of the large computational power required for heat exchanger circuitry optimization. In this study, the optimization procedure is based on a genetic algorithm (GA), which is a specific type of evolutionary algorithm. GAs belong to a family of derivative-free optimization methods inspired by the natural evolution process [12–14], and are widely employed in engineering optimization problems. Their derivative-free nature allows for the exploration of non-trivial, non-convex, or high-dimensionality search spaces without requiring gradient information, making them suitable for problems in which the objective function is not differentiable or approximating derivatives is computationally expensive [13,14]. Introduced in the 1970s [12], GAs operate through an iterative process that mimics the evolution of a population by natural selection; specifically, a population of candidate solutions is transformed over successive iterations (named generations) using selection, crossover, and mutation operators, progressively improving the objective function [15–17] and mimicking natural processes. Other advantages of GAs are their inherent parallelizability and ability to reduce the risk of being trapped in local minima. Nonetheless, theoretical convergence guarantees are generally weak and premature convergence may occur [13,14]. Although this work focuses on single-objective optimization, GAs can also be naturally extended to multi-objective optimization problems, in which they approximate the Pareto front [18–20]. These characteristics make GAs powerful and flexible tools for addressing a wide range of engineering and design optimization problems, such as building design [21,22], industrial component design [23,24], and composite material optimization [25,26].

Evolutionary algorithms have been broadly investigated for heat exchanger circuitry optimization in recent studies. Studies include the pioneering work of Domanski [27] and the development of a public-domain simulation platform to analyze finned-tube evaporators and condensers in relation to refrigerant circuitry arrangements [28,29], evolving to more sophisticated models [30–35] and algorithms [36–40], with the most recent efforts [41–44] enabling the direct use of genetic operators in an unrestrained search space of complex circuitry with arbitrary numbers and locations of splitting nodes.

Contextually, the stochastic and random features of the search algorithm often yield complex circuitry characteristics following the optimization procedure and may be sensitively affected by deviations in the heat transfer and friction models. Accordingly, not only the accuracy of the numerical model but also the optimized circuitry characteristics and their benefits should be physically interpreted [45–47] and experimentally verified. However, the extensively available results in the literature are not consistently accompanied by experimental verifications.

Validation of the simulation models themselves has been limited. A few exceptions include, for instance, [45,48], where manufacturer test data for a unit operated both in cooling and heating modes were used to validate the simulation model by demonstrating deviations in the cooling energy efficiency ratio and heating coefficient of performance (COP) below 6 %. Nonetheless, this provides only indirect validations of the heat exchanger models, without possibility to directly verify heat transfer coefficient and pressure drop formulations. Other studies, such as [32,41], validated their models against limited experimental datasets for two-phase and single-phase refrigerant conditions, respectively.

Even more scarce are experimental evaluations of the optimized circuitry characteristics or the verification of the benefits claimed from optimized designs. To the authors' knowledge, only [49,50] provided some experimental evidence. Specifically, experimental investigations of the effect of circuitry branching were conducted in [49], in which a reversely variable circuitry was proposed to balance the optimized requirements for both the condenser and evaporator operations of the same finned-tube heat exchanger. The effect of the circuit number was studied using EVAP-COND 4.0, suggesting a four-circuit configuration for the evaporator and two-circuit merging into one configuration for the condenser. Experimental tests demonstrated that the two-to-one circuit configuration exhibited a 6.1 % higher cooling capacity than the four-circuit configuration, and the latter had a 3.9 % higher heating capacity than the 1.5-circuit configuration when reversely operated. In addition, [50] manufactured and tested an optimized heat exchanger. Nonetheless, the measured capacity and COP improvements were relatively small (a 2.2 % increase in capacity and 2.9 % increase in COP) and burdened with a measurement uncertainty up to 1.1 %. Other studies have reported case-specific validations of circuitry enhancements. For example, Ma et al. [44] experimentally demonstrated that sequentially merging the circuits of a small-tube condenser can achieve EER and COP levels comparable to those of standard tube sizes, while reducing material cost and refrigerant charge by approximately 20 % and 12 %, respectively. In another effort, Sim et al. [51] introduced and verified the concept of variable circuitry heat exchangers (VCHX), designed to improve off-design performance under partial-load conditions. More recently, Xiong et al. [52] showed that selecting appropriate circuit designs for vapor-bypassed heat exchangers can yield notable performance gains in reversible air-source heat pumps, with experiments confirming a 4.0 % increase in the annual performance factor (APF). It can therefore be observed that the effectiveness of evolutionary algorithms for circuitry optimization has yet to be fully verified. In response, this study proposes highly manufacturable and efficient circuitry designs and presents experimental work aimed at validating the performance of genetic programming applied to heat-exchanger circuitry optimization. Following a comprehensive validation of the numerical model, the study also confirms the benefits associated with the optimized circuitry features. The remainder of this paper is organized as follows: Section 2 describes the numerical and experimental methods used to identify, analyze, and test optimized circuitry designs for the evaporator of an R32 unit; Section 3 presents and discusses the verification results, including model accuracy, optimized circuitry characteristics, and the performance improvements achieved through the optimization algorithm. The evidence provided supports the development of reliable numerical tools and demonstrates the practical applicability of genetic programming for efficient product development.

2. Materials and methods

2.1. Genetic programming for circuitry optimization

The circuitry optimization procedure was based on a tube-by-tube numerical model subject to uniform air distribution, where the heat transfer and pressure drop on both the air and refrigerant sides were modeled using the correlations summarized in Table 1. For each candidate circuitry and fixed air-side geometry, the simulator evaluates performance under the boundary conditions and operating requirements

Table 1
Summary of the correlations adopted in the numerical model.

	Airside	Refrigerant	
		Single-phase	Two-phase
Heat transfer coefficient	Wang [53]	Dittus-Boelter [54]	Shah (1982) [55]
Fin/Tube pressure drop	Wang [53]	Blasius	Müller–Steinhagen and Heck [56]
U-bends pressure drop	–	Popiel and Wojtkowiak [57]	Domanski and Hermes [58]

listed in Table 2. The simulator inputs include the return-air temperature, the compressor isentropic and motor efficiencies, and the refrigerant enthalpy entering the evaporator, which is defined by the condensing temperature and degree of subcooling. The model iteratively solves for the local refrigerant state and mass flow rate in each tube, as well as the total refrigerant flow rate and inlet pressure required to satisfy the specified cooling capacity and superheat conditions while maintaining heat and mass balance throughout the circuitry. These calculations must accommodate multiple outlets, parallel branches, and splitting nodes; in such cases, the simulator enforces equal pressure at all outlets and equal vapor quality at the downstream nodes of any two-phase splitting junction. The resulting solution provides a complete description of heat-exchanger performance and, when combined with the assumed condensing temperature and compressor efficiencies, yields an estimate of the corresponding cycle COP. Details of the mathematical formulation and numerical implementation can be found in [35,41,42,45].

Optimization problems are widely reliant on evolutionary algorithms because of their effectiveness in obtaining robust solutions in complex search spaces. The optimization algorithm adopted in this study was described in [44,45] and relies on the fundamental concepts of graph theory and genetic programming, respectively, for recognizing unfeasible features and applying genetic operators to an unrestrained search space of complex circuitries with arbitrary numbers and locations of splitting nodes. Genetic programming is a path generation algorithm that applies genetic operators to tree structures that are used as genotypes. In such tree structures, nodes correspond to tubes and are generated according to rules designed to exclude unfeasible circuits, such as closed loops, merging from opposite sides of the heat exchanger, disconnected tubes, or excessively long U-bends [44]. Each tree represents a circuit. It starts with the root nodes and ends with the leaves, corresponding to the inlet and outlet tubes, respectively. A tree can branch into subtrees by splitting and merging nodes. The depth of a tree is equal to the number of nodes that must be traversed from the root node to reach the leaf.

The proposed genetic algorithm involves five main stages:

(a) initialization: a population of starting tree structures (hereafter also referred to as "individuals") is randomly generated;

(b) selection: the individuals are evaluated on the basis of a fitness function (hereafter also referred to as "objective function"), with a fixed number of the best ones being selected and the remaining ones discarded;

(c) crossover: among the individuals selected during the previous step, pairs of "parent individuals" are sampled and used to generate new individuals (i.e., new tree structures), also referred to as "offspring," according to suitable crossover operators;

(d) mutation: additional offspring are generated by randomly sampling individuals from the selected population and/or the offspring, and perturbing them through a suitable mutation operator;

(e) new generation creation and application of topology and manufacturability constraints: this step creates a new population of post-processed individuals, composed of offspring plus a percentage of selected parent individuals (the "elitism" procedure), ensuring that the corresponding tree structures adhere to the physical and manufacturability requirements.

These five stages are iteratively repeated (each iteration is denoted as a "generation") until a stopping criterion is reached.

In particular, the applied search process is characterized by a selection phase based on the roulette wheel method [59], where the likelihood of an individual being chosen as a parent is proportional to its fitness value. Moreover, genetic-like operations, i.e., crossover and mutation, are applied to the parent circuits to obtain new offspring circuits, according to the criteria described in [41,42]. The main stages are repeated until the optimization criterion is satisfied, or maximum number of generations is reached. The search for refrigerant circuitries approaching the maximal COP was performed for a 36-tube evaporator with 12 tube rows and the transfer surface features (Fig. 1) of the manufactured baseline heat exchanger (Table 3). Specifically, corrugated fins and smooth tubes were used.

For a given cooling capacity, the COP can be maximized by minimizing the compressor work. Under the calculation conditions listed in Table 2, the maximum cycle efficiency can be approached by searching for circuits that can maximize the evaporator outlet pressure (Eq. 1).

$$COP = \frac{\dot{Q}_e}{W_{com}} \quad , \quad COP_{cycle,max} \rightarrow W_{com,min} \rightarrow P_{e,out,max} = P_{e,in,opt} - \Delta P_{e,opt} \tag{1}$$

In addition to improving the thermal matching between the refrigerant and air temperature distributions, the evaporator outlet pressure can be increased by optimizing the balance between pressure drop and heat-transfer coefficient, which directly affects the mean temperature difference between the two fluids. In a previous study [45], the authors demonstrated that this could be achieved by minimizing the corresponding irreversible thermodynamic losses, namely the entropy generation arising from friction and that related to finite-temperature-difference heat transfer.

The optimization runs, conceptually represented in Fig. 2, adopted a population size of 500 with 100 generations. The elitism probability defines the number of best-performing genes (rounded down to the nearest integer) to be carried to the next generation; in this case, 500 × 0.005 circuitries. Therefore, 500 × 100 × (1–0.005) = 49,750 circuitries were investigated for each optimization case according to the algorithm settings listed in Table 4.

The computational cost for each optimization case was 91 h for a PC unit with an Intel(R) Core(TM) i5–9500 CPU 3.00GHz processor and 8.00 GB of installed RAM. Fig. 2 conceptually illustrates the search for the optimized heat transfer and pressure drop characteristics of the heat exchanger circuitry. The evolutionary algorithm acts not only on patterning features to generate suitable matching between the airside and refrigerant-side temperature distributions, but also on branching features to limit the pressure drop and control the local refrigerant mass flux and heat transfer coefficient, here related to the logarithmic mean temperature difference (LMTD). The optimization results are illustrated in Fig. 3 and indicate the ability of the proposed optimization method to define suitable features of the refrigerant circuitry for different

Table 2
Operating conditions.

Parameter	Value
Air inlet temperature (return air from the room)	26.0 °C
Air inlet velocity	2.0 m/s
Air inlet pressure	101,325 Pa
Refrigerant	R32
Superheating degree	5.0 °C
Cooling capacity	3.0, 3.5, 4.0 kW
Condensation temperature	35.0 °C
Subcooling degree	5.0 °C
Compressor isentropic efficiency	85 %
Electric motor efficiency	85 %
Residual convergence tolerance	1×10^{-6}

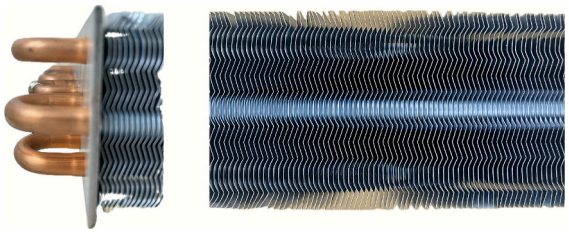

Fig. 1. Upper side view of the heat exchanger showing the finned-tube features.

Table 3
Structural features of the evaporator.

Parameter	Value
Tube outer diameter	6.4 mm
Tube inner diameter	5.4 mm
Tube length	0.5 m
Tube vertical pitch	19.1 mm
Tube transversal pitch	16.0 mm
Fin spacing	1.2 mm
Fin thickness	0.12 mm
Total height	0.267 m
Frontal area	0.133 m^2
Fin corrugation amplitude	1.2 mm
Fin corrugation pitch	8.0 mm
Fin corrugation angle	29.1 °

refrigerants and operational requirements. In the schematic, outlet tubes are indicated by "O" symbols, inlet tubes by "I" symbols, and splits by "S" symbols. The solid and dashed lines represent the U-bends at the rear and front sides of the heat exchanger, respectively. In general, the patterning features were consistent for the three capacity requirements, resulting in a cross-parallel arrangement consistent with the decreasing saturation temperature by pressure drop along the two-phase refrigerant flow, followed by a cross-counter flow pattern to exit the heat exchanger and match the superheated areas of the heat exchanger.

The circuitry optimization performed at 3.0 kW yielded a single-inlet, two-outlet branching configuration with a split junction located at the eighth tube depth from the inlet. The circuitries optimized for 3.5 and 4.0 kW operation exhibited branching configurations with two and three parallel circuits, respectively. Finally, to accommodate the additional manufacturability limitations currently required by the industry, the circuitry was simplified as shown on the right-hand side of Fig. 3, while maintaining patterning and branching characteristics with minor to no (<0.5 %) COP deficits compared with the optimized circuitry from the optimization algorithm (Fig. 4). Specifically, an upward and balanced splitting junction, a gravitationally favorable flow, and tube bends only on the rear side of the heat exchanger were the additional features satisfied by the manufactured heat exchangers tested in this study. Correspondingly, the splitting at the eighth tube depth of the optimized circuitry at 3.0 kW, and the two and three branches of the optimized circuitries at 3.5 and 4.0 kW, respectively, were maintained. In addition, the optimized patterning featuring cross-parallel flowing at the beginning of the circuit and cross-counter towards the outlet were consistently maintained throughout this operating range.

The performance of the optimized circuitries when simulated over a capacity range of 3.0 to 4.0 kW is illustrated in Fig. 4. The top of the figure shows the COP values of the circuitries resulting from the optimization algorithm when simulated at the capacity requirements shown in the label in the top-right corner. The bottom shows the design performance variation ΔCOP of the corresponding circuitries when modified to satisfy the additional manufacturability constraints. It can be observed that the adjustment of the flow complexities, which pose challenges in manufacturability, did not significantly affect the resulting performance, thereby supporting the significance of the optimized patterning and branching features.

In addition, in the selected range of operational conditions, the patterning features predominantly influenced the optimal

Table 4
Optimization search settings.

Parameter	Value
Population size	500
Number of generations	100
Crossover probability	0.80
Mutation probability	0.005
Elitism probability	0.005

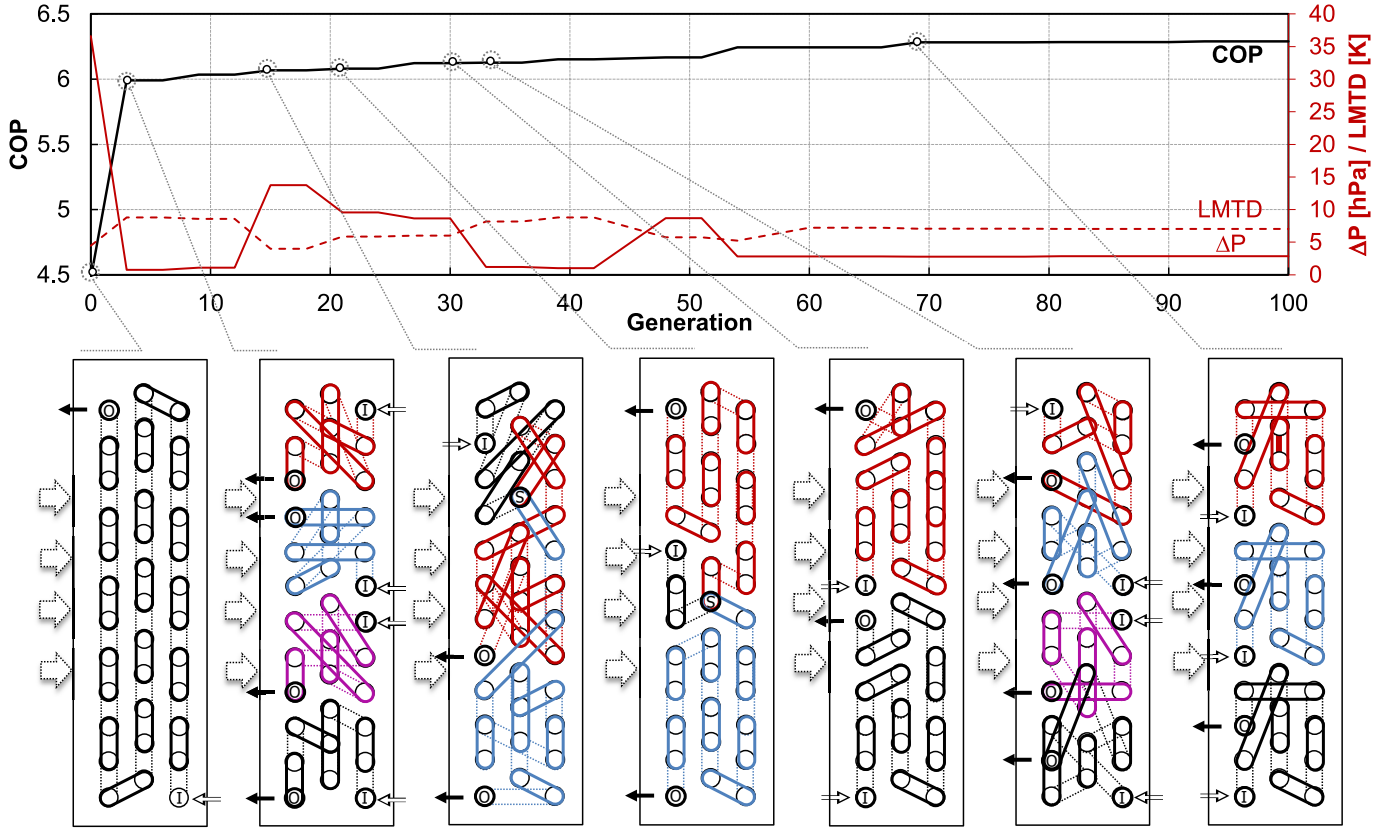

Fig. 2. Conceptual progression of the genetic programming algorithm for COP optimization.

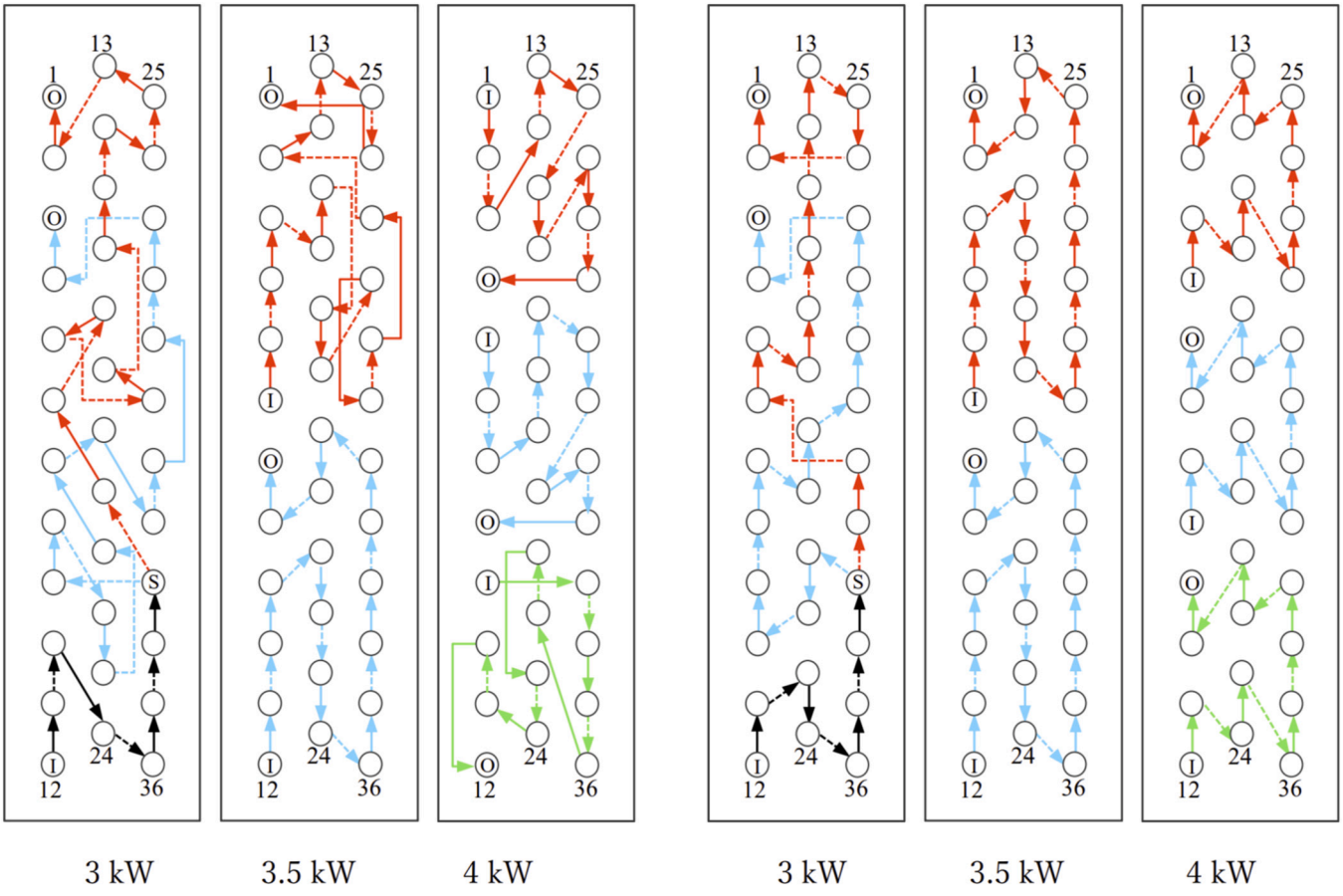

Fig. 3. Resulting optimized circuitries (left) and corresponding simplifications to comply with manufacturing constraints (right) for 3.0, 3.5, and 4.0 kW.

characteristics of the heat exchanger. This observation is related to the relatively large exchange surface and limited pressure drop, which limit the impact of branching. Accordingly, the circuitries optimized at lower capacity conditions (3.0 to 3.5 kW) demonstrated larger benefits at partial load operation and lower deficits at larger load operation compared with the circuitries optimized for full load operation (4.0 kW).

Previous numerical studies employing this optimization approach have shown that the optimal circuitry configuration depends strongly on the thermophysical and transport properties of each refrigerant. In particular, the optimization results were highly sensitive to factors such as the temperature glide of non-azeotropic mixtures, the magnitude of the latent heat of vaporization, and the evaporating pressure. Future work will focus on validating the model's accuracy and assessing the performance gains achievable when the methodology is applied to low-GWP refrigerant alternatives.

2.2. Manufactured heat exchangers

To verify the simulator accuracy and effectiveness of the optimization algorithm through the effect of the optimized patterning and branching characteristics, the circuitries optimized at 3 and 4 kW capacities were manufactured and tested, and their performance and operating characteristics were compared with a baseline circuitry representing the reference patterning and branching features of evaporators. In fact, the cross-parallel patterning is reasonably aligned with the decreasing saturation pressure owing to the pressure drop and with the condenser features when operated in a reversed flow for heating operation, suggesting the advantage of the cross-parallel pattern in maintaining a moderate temperature difference.

Fig. 5 shows a schematic side drawing of the baseline heat exchanger with cross-parallel circuitry with two circuits. Although it may be arbitrary to define a reference heat exchanger circuitry, the selected circuitry is a recurrent selection for the evaporators of current systems. Reversible systems would operate with a counter-flow condenser resulting from the reverse operation of the baseline evaporator circuitry. In addition, the two-branch evaporator exhibits a reasonably low pressure drop.

Fig. 6 shows the bends on both sides of the two optimized heat exchangers. The performances of the manufactured heat exchangers were investigated over a range of required cooling capacities, representing partial load operation. Fig. 7 presents the simulation results and highlights the performance improvements achieved using the optimized circuitries.

The investigation of the off-design operation suggests that circuitries optimized at partial load operation (such as Opt.#3 kW) showed a minimal deficit compared with the circuitry optimized at full load operation (Opt.#4 kW) and more substantial benefits at partial load operation; hence, it is necessary to consider partial load operation during the optimization phase to maximize the advantage of optimized heat exchangers over seasonal operation.

Accordingly, Fig. 8 shows the effects of different circuitries on the operating conditions of the refrigerant, which determine the performance of the system. As the cycle COP at a given cooling capacity was maximized for the maximal outlet evaporator pressure, Fig. 8 depicts the refrigerant pressure of the flow along the circuitry for the three manufactured units at 3 and 4 kW operation. For ease of comparison and interpretation, all tubes were considered when defining the flow depth. Specifically, the tubes had equivalent flow depths in circuitries with multiple circuits from the splitting node. Accordingly, the maximum outlet pressure could be achieved using the units designed under the corresponding operating conditions.

Specifically, it can be observed that at 3.0 kW operation (left-hand

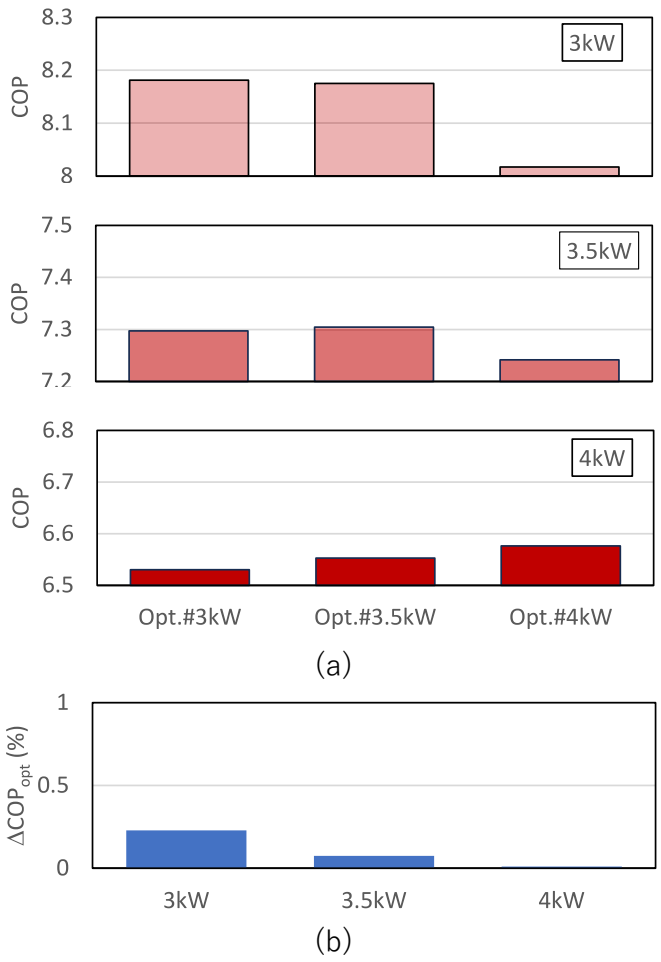

Fig. 4. Performance of optimized circuits for off- and on-design conditions (a) and relative performance deficits of the circuitries simplified considering manufacturing constraints (b).

side of Fig. 8) the three-circuit circuitry optimized at a full load (Opt.#4 kW) underperformed owing to a lower heat transfer coefficient arising as a consequence of the smaller local refrigerant flux, which decreased the pressure drop, but was not sufficient to compensate for the requirement of a lower inlet saturation pressure and larger average temperature difference between the refrigerant and air. Consequently, the circuitry optimized at a partial load (Opt.#3 kW) achieved a higher outlet pressure and better COP (Fig. 7). Complementary considerations can be extracted from the results obtained at 4.0 kW operation (right-hand side of Fig. 8), where the larger inlet saturation pressure achieved by a better heat transfer coefficient of the circuitry optimized at a partial load (Opt. #3 kW) could not compensate for the substantially larger pressure drop, and the circuitry optimized at a full load eventually operated at a higher outlet evaporator pressure.

2.3. Experimental setup

To verify the performance and benefits of the optimized circuitries, experiments were conducted using dedicated equipment constructed to collect the experimental performance data of the corresponding heat exchangers within an air-conditioning cycle. A schematic of the structure and instrumentation of the equipment is shown in Fig. 9.

The apparatus featured two main sections: one representing the outdoor heat exchanger and the other representing the indoor heat exchanger. Each was installed in a dedicated psychrometric chamber to steadily control the inlet airstream velocity, temperature, and humidity in the condenser and evaporator. Correspondingly, the airside temperature, humidity, and airflow rate were measured using the auxiliary sensors of a certified testing facility [60]. Refrigerant pipelines were insulated with 13 mm-thick Ethylene Propylene Diene Monomer (EPDM). The specifications of the main components and instrumentation used in the test are summarized in Tables 5 and 6, respectively.

While the R32 refrigerant circulated in the refrigerant circuit, the indoor heat exchanger was also evaluated by calculating the measured supplied cooling capacity using the air enthalpy method, thereby collecting and rectifying the airflow through a measuring chamber and measuring the downstream temperature, humidity, and airflow rate.

Test runs of the apparatus were conducted to verify the operational

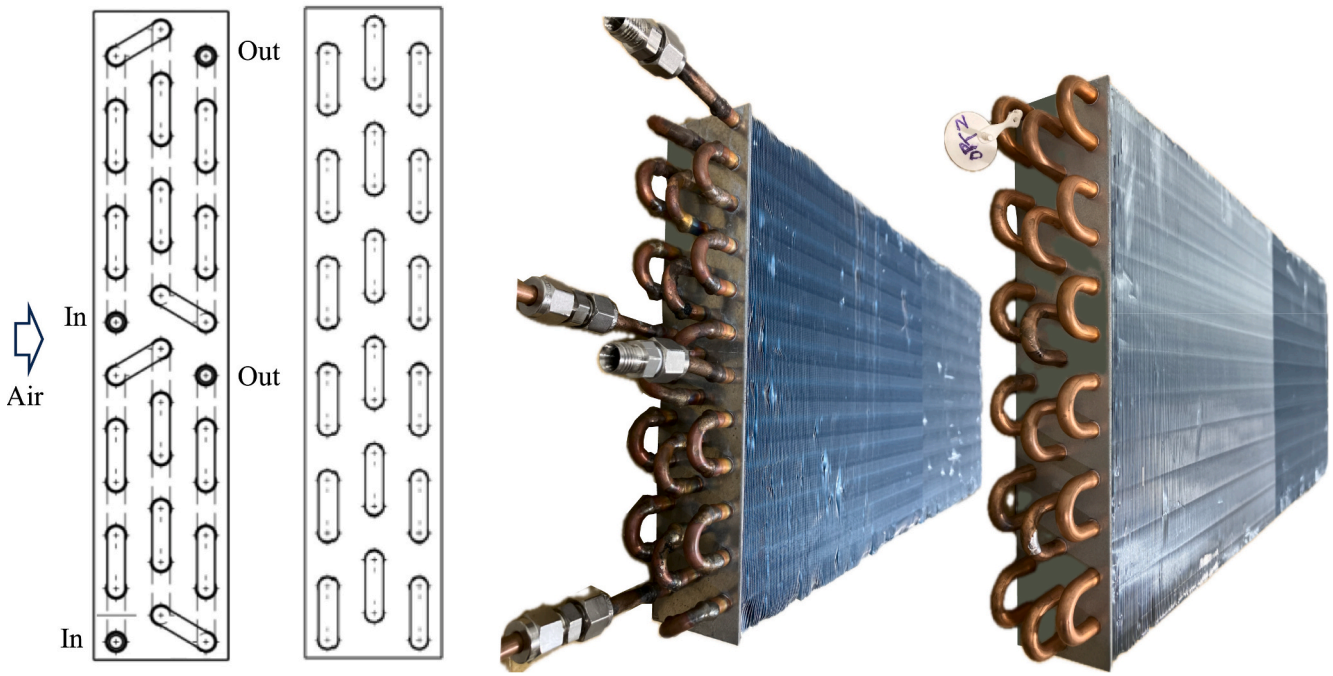

Fig. 5. Schematics of side view and photographs of the manufactured baseline heat exchanger.

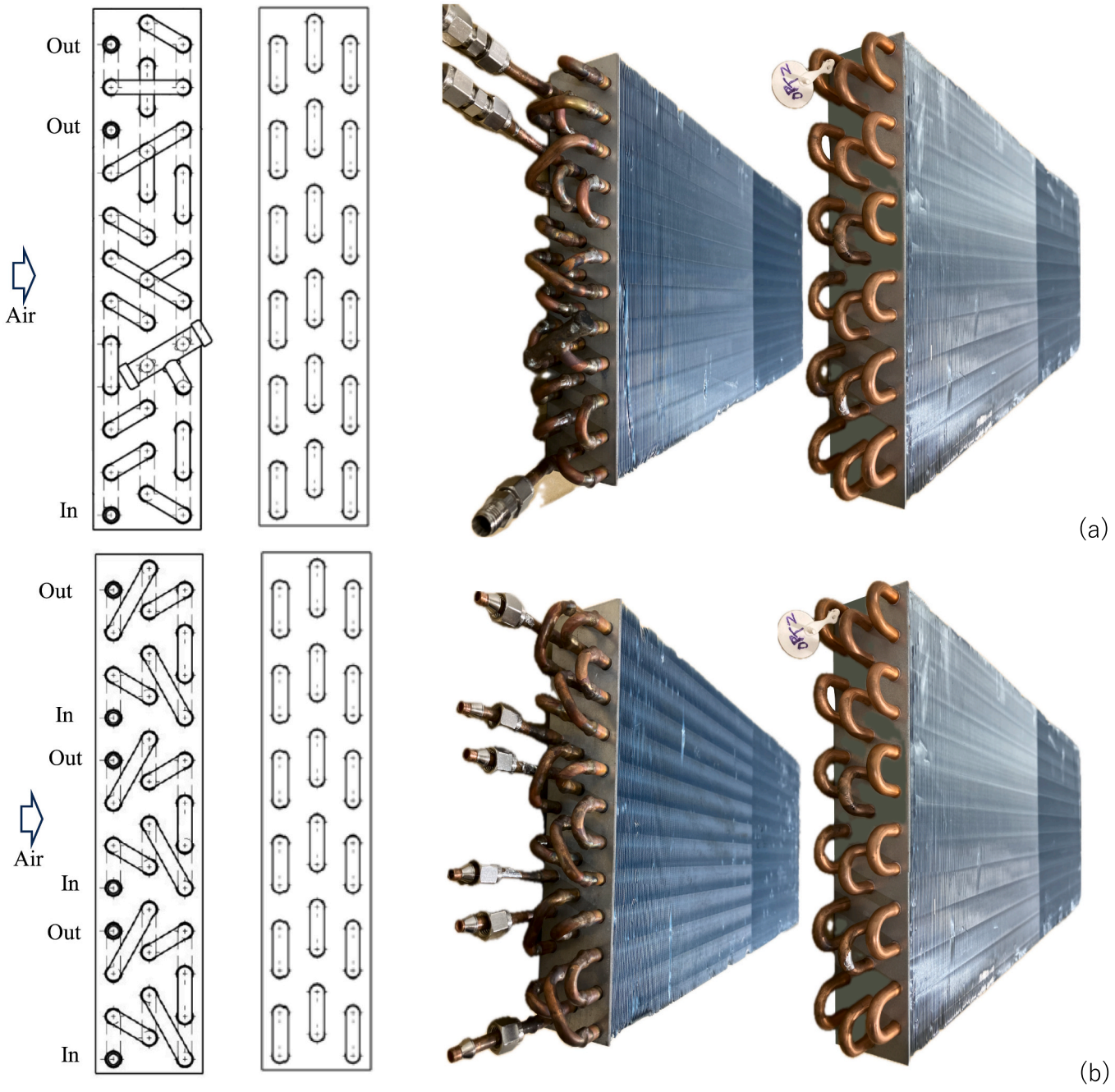

Fig. 6. Schematics of the side view and photographs of the manufactured Opt.#3 kW (a) and Opt.#4 kW (b) heat exchangers.

methods for adjusting the experimental conditions. Specifically, the main cycle variables were the cooling capacity and enthalpy at the evaporator inlet, which were adjusted via the following procedures. The cooling capacity was adjusted by manually controlling the compressor rotational speed via the inverter frequency, whereas the evaporator inlet enthalpy was varied by adjusting the condenser subcooling through the refrigerant charge. Refrigerant inlet and outlet enthalpy at the evaporator were measured with dedicated temperature and pressure sensors, while the refrigerant flow rate was acquired in subcooled state before the expansion valve. Consequently, the airside boundary conditions were controlled using the reconditioning equipment of the psychrometric chamber. The outdoor ambient temperature and airflow were set to control the condensation temperature. The indoor airflow rate in the evaporator was adjusted under different capacity conditions to maintain the evaporating temperature within a reasonable operating range. In addition, the degree of superheating was controlled by manually adjusting the expansion valve opening, and the discharge temperature at the compressor was limited by the use of liquid injected through manually adjusting the needle valve opening. Liquid refrigerant from the liquid line upstream of the mass flow meter was collected in the liquid tank and released upstream of the compressor's suction port. Finally, the oil return amount was controlled by manually adjusting the needle valve opening of the oil return pipe from the oil separator.

3. Results and discussion

3.1. Experimental results

Measurements were taken every 5 s, and the average values over a 1-min period—after the refrigeration cycle had stabilized—were used for

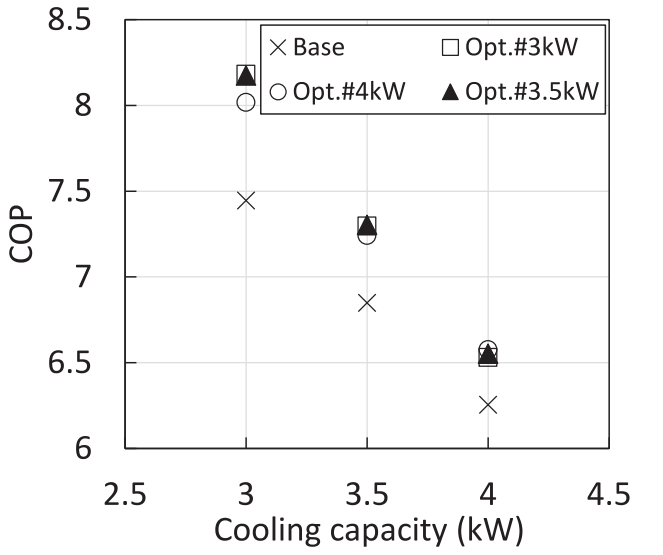

Fig. 7. Calculated performance of the manufactured heat exchangers for off- and on-design conditions.

data reduction. The heat exchangers were tested in cooling operation under 27 °C dry-bulb and 19 °C wet-bulb indoor air conditions, with 29 °C dry-bulb and 19 °C wet-bulb outdoor air temperatures. The test equipment was designed to meet the airflow-uniformity requirements specified for open refrigerated display cabinet testing [61], ensuring a highly uniform air distribution within the psychrometric chamber. Different datasets were collected with the evaporator air velocity set to approximately 1.6 m/s for a target cooling capacity of 3.0 kW and approximately 2.0 m/s for 4.0 kW, except for a few cases in Figs. 10–11 where the capacity between 3 and 4 kW was adjusted at a fixed air velocity by modulating the compressor speed. In addition, the evaporator superheat was adjusted to an approximate target temperature of 10 K and then varied to lower values. Finally, the degree of subcooling in the condenser was varied between 1 and 20 K. During the cooling operation, the data were measured for the three heat exchangers that were used as evaporators.

The complete set of measurement results are summarized in Tables S1-S6 of the supplementary material. While adjusting compressor speed to achieve approximately 3 kW cooling capacity, the given air velocity and degrees of superheating/subcooling define resulting pressure drop, evaporation temperature at mid pressure, and outlet refrigerant pressure. Accordingly, Figs. 10 and 11 present the key measures extracted from the data for 3- and 4-kW operation, respectively.

Direct uncertainties were evaluated as the standard deviation associated with the measured values, considering only sensor accuracy. Uncertainties of the temperature u_T, pressure u_p, and pressure drop $u_{\Delta p}$ measurements were ± 0.29 K, 0.22 kPa, and 13 kPa, respectively. The uncertainties of the derived performance parameters were then calculated by propagating the individual sensor uncertainties as in Eq. (2). Here, $h_{e,i}$ and $h_{e,o}$ represent the outlet enthalpy of the evaporator, respectively. As clarified below, this formulation assumes identical condensation temperatures and compressor efficiencies, thereby limiting uncertainty propagation to the measured parameters at the evaporator inlet and outlet.

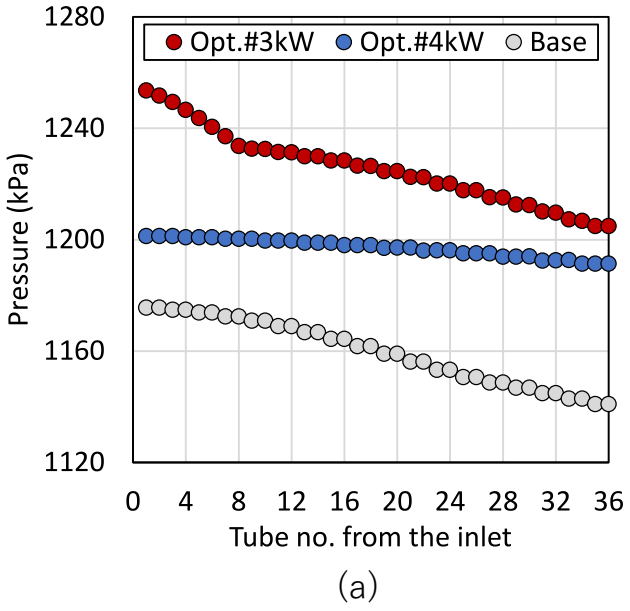

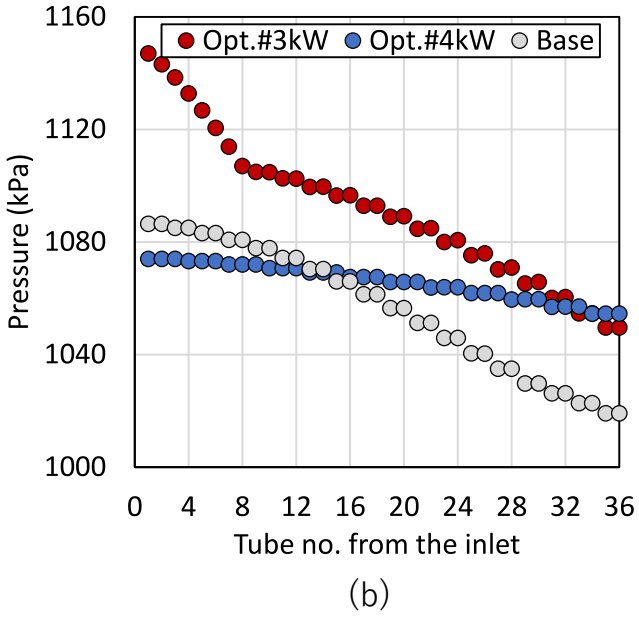

Fig. 8. Simulated pressure variation along the three manufactured circuitries for (a) 3-kW and (b) 4-kW operation.

Fig. 12 shows a comparison of the pressure drop and evaporation temperature for data with similar condenser outlet subcooling from the three heat exchanger circuitries. While the temperature measurements exhibit visible sensor uncertainties, the error bars for the differential pressure measurements are extremely small and are obscured by the marker size. Compared with the baseline circuitry, Opt.#4 kW exhibited a lower pressure loss and higher evaporation temperature (average

$$u_{COP} = \sqrt{\left(\frac{\partial COP}{\partial h_{e,o}}\frac{\partial h_{e,o}}{\partial T}\right)^2 u_T^2 + \left(\frac{\partial COP}{\partial h_{e,o}}\frac{\partial h_{e,o}}{\partial p}\right)^2 u_p^2 + \left(\frac{\partial COP}{\partial h_{e,i}}\frac{\partial h_{e,i}}{\partial T}\right)^2 u_T^2 + \left(\frac{\partial COP}{\partial h_{e,i}}\frac{\partial h_{e,i}}{\partial p}\right)^2 u_p^2} \quad (2)$$

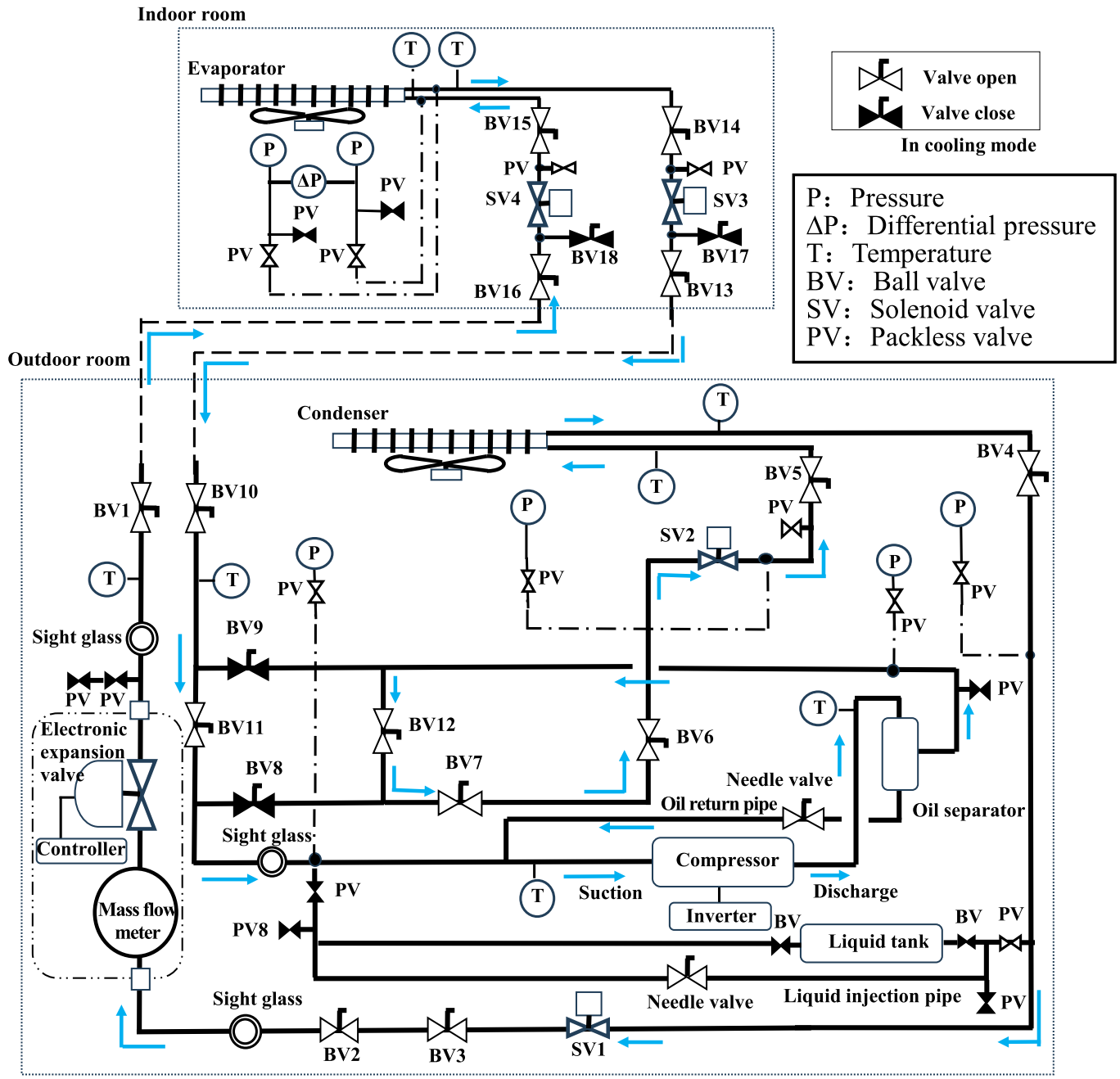

Fig. 9. Schematic of the structure and instrumentation of the testing equipment.

Table 5
Equipment specifications.

Component	Specifications
Horizontal scroll compressor	15.9 cc Stroke volume, POE lubricant, 25–100 rps rotational speed range.
General purpose inverter	C1-022LF2, (Hitachi Industrial Equipment Systems).
Expansion valve	PKV-14BS, 0.05 Cv value, 480 pulses max opening, (Saginomiya Seisakusho).
Expansion valve controller	YNE-SN20, Refcon Controller, (Saginomiya Seisakusho).
Condenser fan	EMR1865-A, (× 2 units) 8.2 m^3/min Maximum airflow, (Oriental Motor).
Liquid receiver tank	500 cc capacity, (Swagelok).
Piping	ϕ12.7 mm Diameter, 0.8 mm wall thickness.
Pipeline insulation material	13 mm-thick Aeroflex material.

Table 6
Instrumentation.

Sensor	Specifications	Range	Accuracy
Mass Flow Meter	ALTImass II Type U, (Oval Corporation)	18–360 kg/h	±0.1 % of reading
Pressure Sensor	FP101, (Yokogawa Electric Corporation)	0–5 MPa	±0.25 % of full scale
Pressure Gauge	EJX110J, (Yokogawa Electric Corporation)	2.5–500 kPa	±0.075 % of full scale
Power Meter	WT1804E, (Yokogawa Electric Corporation)	0.375–12,500 W	±0.05 % of reading
Thermocouples	Type T	−200-350 °C	±0.5 K

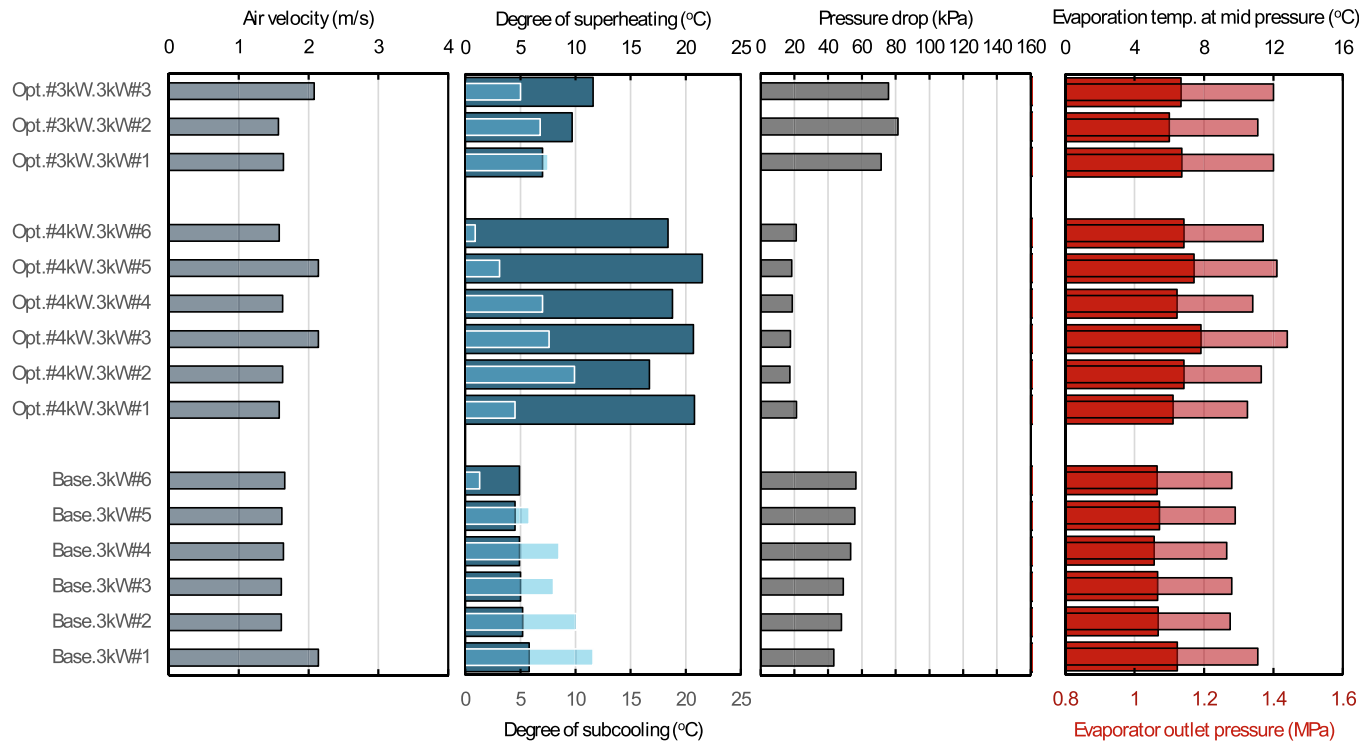

Fig. 10. Experimental air velocity, degrees of superheating and subcooling, pressure dop, evaporation temperature at mid pressure, and outlet pressure for the baseline and optimized heat exchangers at 3 kW capacity operation.

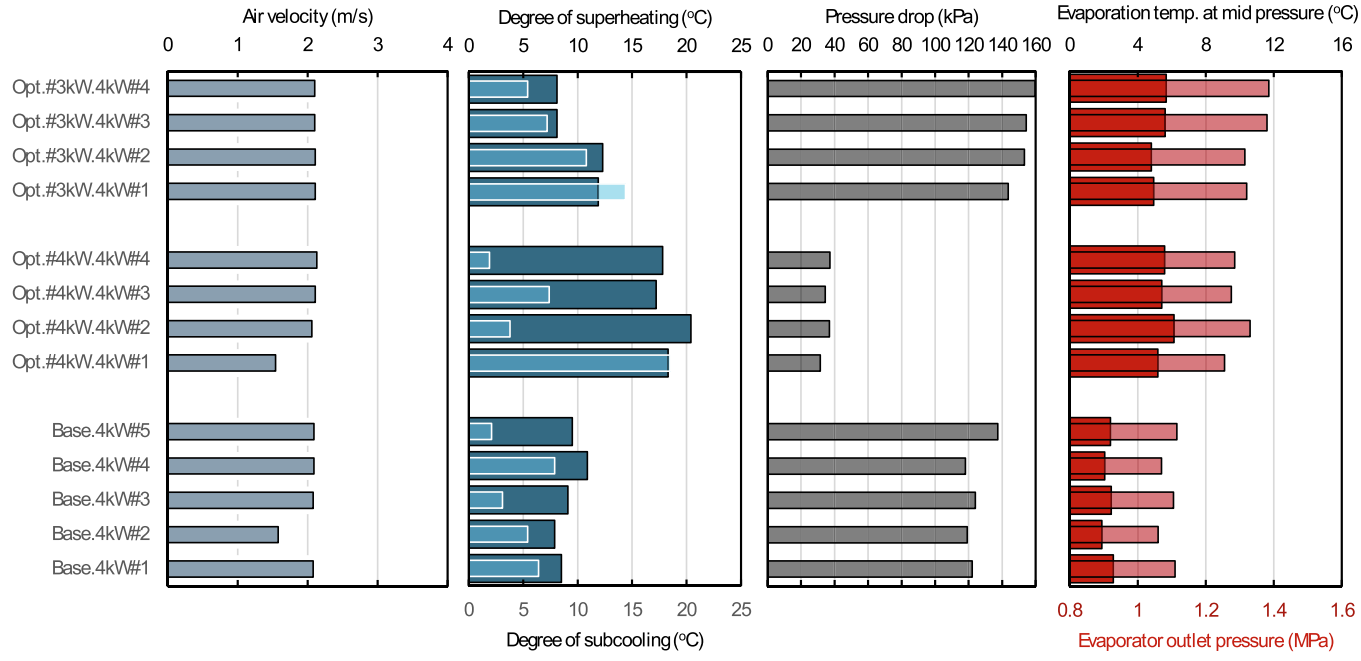

Fig. 11. Experimental air velocity, degrees of superheating and subcooling, pressure dop, evaporation temperature at mid pressure, and outlet pressure for the baseline and optimized heat exchangers at 4 kW capacity operation.

evaporator temperature). In contrast, Opt.#3 kW had a larger pressure loss, and its higher heat transfer coefficient improved the heat exchange efficiency, resulting in a higher (average) evaporation temperature and lower compressor speed. Specifically, the optimized configurations operating at 3- and 4-kW capacities achieved 2.7 and 4.1 K higher inlet saturation temperatures, respectively, combined with a 18.0 kPa

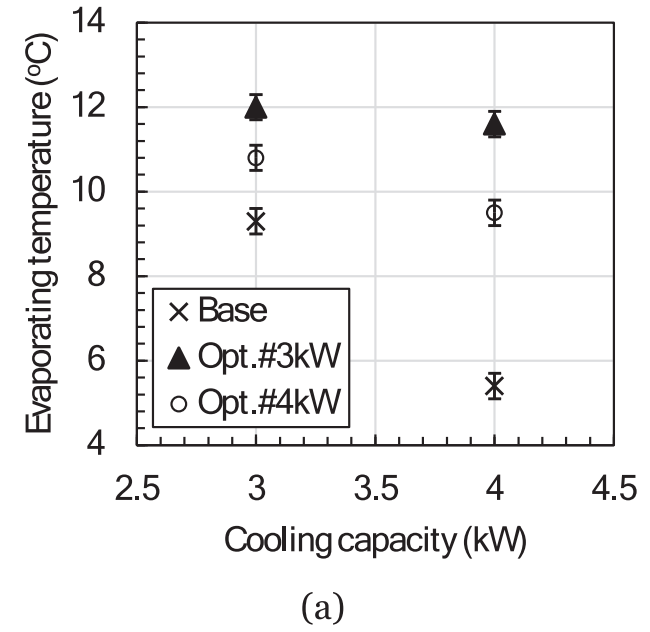

Fig. 12. Experimental evaporation saturation temperature at mid pressure (a) and pressure drop (b) for the three tested neat exchangers.

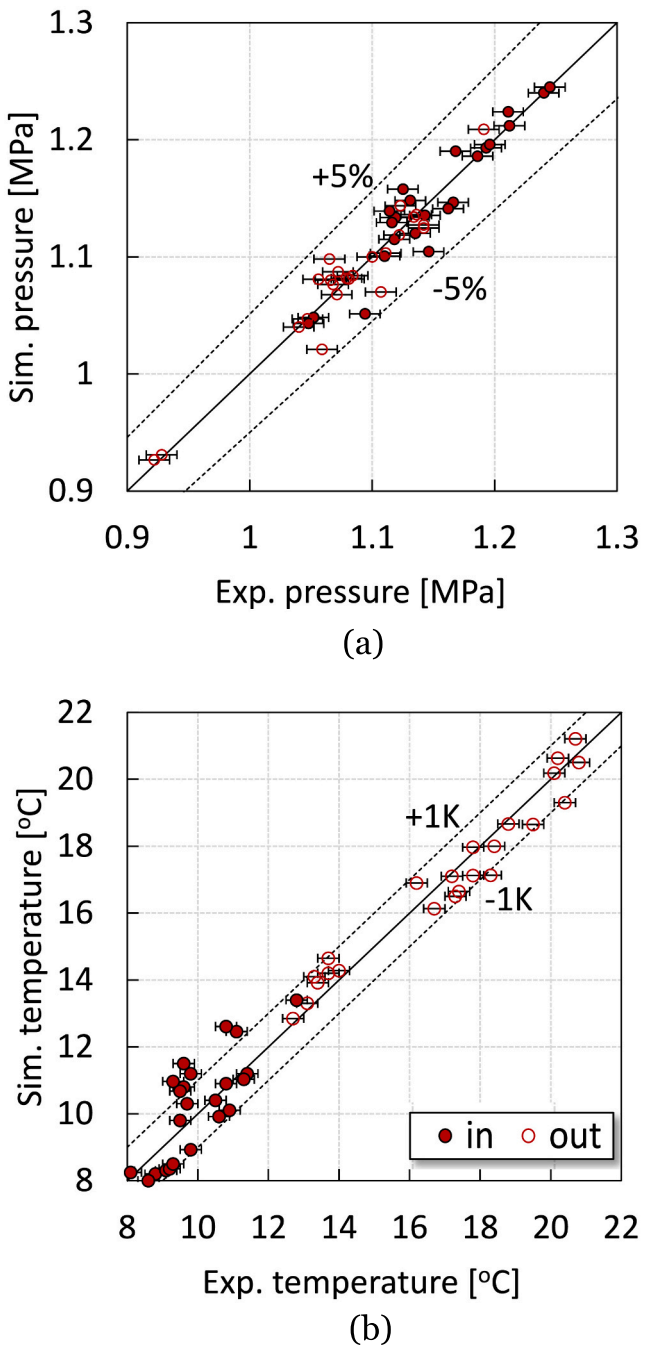

Fig. 13. Accuracy assessment of the pressure (a) and temperature (b) simulation results for conditions corresponding to the experimental data in Figs. 10 and 11.

increase and 83.5 kPa decrease, respectively, in the pressure drop.

3.2. Validation

The collected datasets were used for comparison to validate the numerical model adopted in the simulator. Accordingly, simulations were performed under the corresponding airside inlet conditions, cooling capacity, degree of subcooling and superheating, and condensation temperature.

Fig. 13 demonstrates that the model accurately represented the frictional pressure drop and heat transfer in terms of the evaporating temperature level and outlet temperature, with 66.7 % of the temperature deviation within ±1.0 K and pressure deviations within ±5.0 % of the measured values.

Larger deviations may be attributed to residual non-uniformities in the air-velocity distribution or to simplifying assumptions, such as the imposed homogeneity of vapor quality in two-phase flow at splitting junctions. Nevertheless, the satisfactory accuracy of the results indicates that the experimental setup and the manufacturing constraints applied to the splitting junctions effectively minimized the impact of these modeling simplifications. If these testing conditions cannot be guaranteed, or if operating conditions closer to real field applications are to be examined, the model should be refined to account for vertical airflow maldistribution and for horizontal tube segmentation to represent horizontal maldistribution—albeit at the cost of increased computational effort.

Given that liquid injection is used to limit the compressor discharge temperature—thereby introducing a mismatch between the mass flow rates circulating through the condenser and the evaporator—a

consistent basis for experimental performance comparison is required. Accordingly, the cycle COP values reported in Fig. 12, as well as the corresponding performance improvements of the optimized circuitries, were obtained by assuming that the compressor inlet temperature equals the evaporator outlet temperature and that the compressor operates with an isentropic efficiency of 0.80. Consequently, the experimental values and corresponding results from the numerical simulator are compared in Fig. 14 for corresponding condensation temperatures. This approach ensures that the results remain comparable regardless of liquid-injection use, effectively assuming a condenser sized to match the evaporator inlet conditions.

Fig. 15 illustrates and validates the performance improvement achieved by relating it to the ability to supply the same cooling capacity as the baseline circuitry while operating at a higher evaporating pressure.

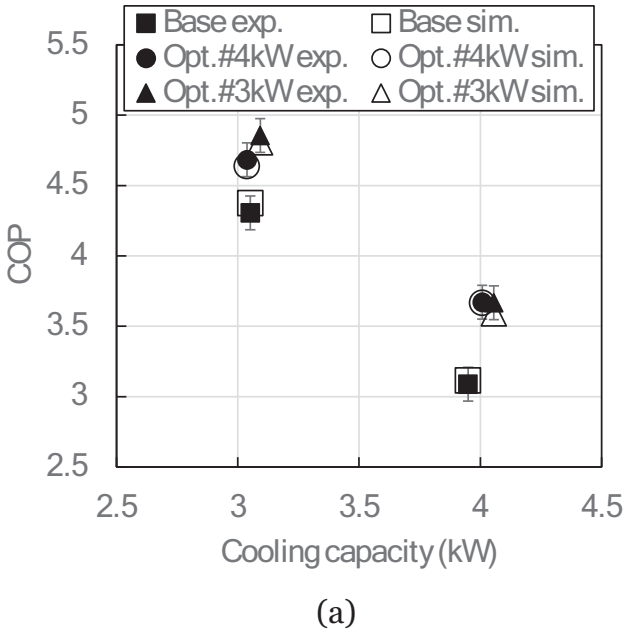

Fig. 14. Validation of the COP (a) and COP improvement (b) achieved by circuitry optimization through genetic programming.

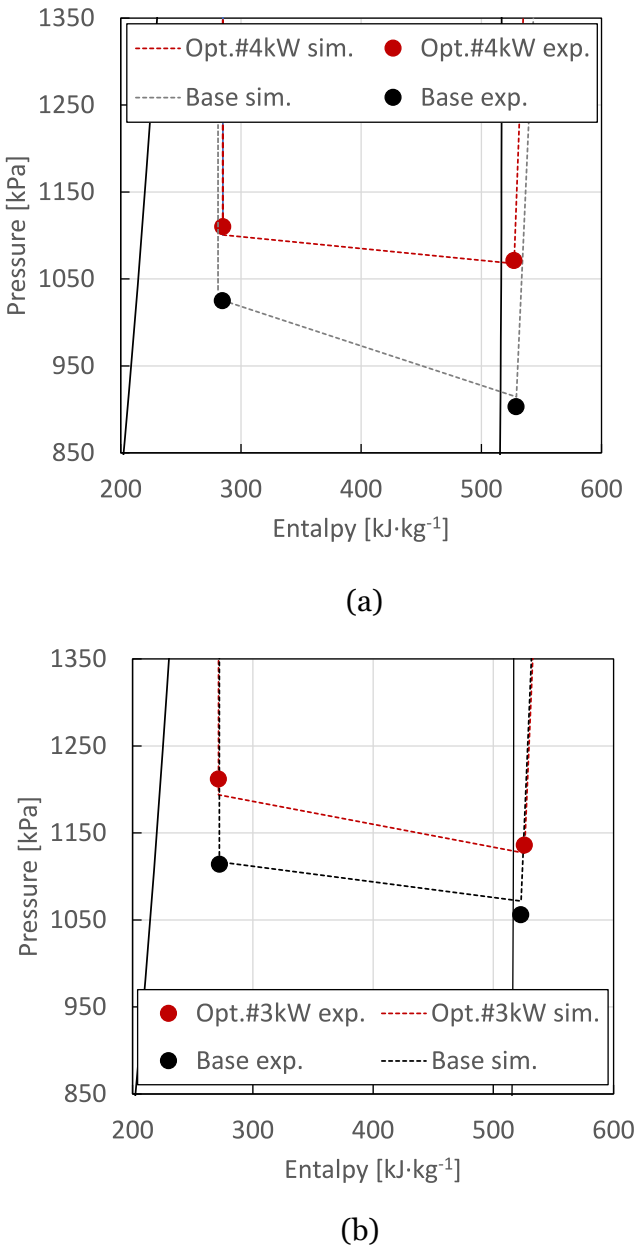

Fig. 15. Validation of enhanced characteristics of the optimized circuitries (a) Opt.#4 kW and (b) Opt.#3 kW in terms of evaporating pressure and resulting pressure drop.

The inlet and outlet states represented in these diagrams are consistent with the experimental measurements plotted as markers. Both the experimental data and numerical results confirm that at 3.0 kW, the Opt.#3 kW circuitry exhibited the highest COP, whereas at 4.0 kW, Opt.#4 kW was the best-performing circuitry.

Accordingly, because these circuitries were optimized to maximize the COP under these conditions, the results were consistent with the design intent. However, although the circuitry Opt.#3 kW had the highest average evaporator temperature at 4.0 kW, owing to its larger pressure loss, the compressor suction pressure was lower, resulting in a 2.1 % lower COP than Opt.#4 kW, in this case, smaller than the propagated experimental uncertainty. As shown in Fig. 14, as a result of the circuitry optimization, the experiments demonstrated an 18.9 % COP improvement at 3 kW and a 12.8 % COP improvement at 4 kW compared with the baseline circuitry. The simulation results consistently highlighted 17.7 % and 9.84 % COP improvements at 3 and 4 kW,

respectively.

4. Conclusion

Evolutionary circuitry optimization is recognized as a cost-effective method for maximizing equipment performance while tailoring its characteristics to a specific refrigerant. However, whether heat exchangers designed using this method can achieve the expected performance when actually manufactured has not been sufficiently verified. This study validated the optimization results and features resulting from genetic programming applied to the circuitry optimization of finned-tube heat exchangers.

The numerical optimization results of the evaporator were identified in terms of optimal branching and patterning characteristics for R32 in a capacity range between 3 and 4 kW and for given airside features. The manufacturability of the optimized solutions was enhanced by introducing additional constraints. Consequently, baseline and optimized heat exchangers were manufactured and tested using dedicated equipment. Test results enabled validation of the numerical model, with temperature and pressure deviations mainly within 5 % of the measured values, as well as the verification of the benefits achievable through optimized branching and patterning. Optimized configurations operating at 3- and 4-kW capacities achieved 2.7 and 4.1 K higher inlet saturation temperatures, respectively, combined with an 18.0 kPa increase and 83.5 kPa decrease in the pressure drop, corresponding to an 18.9 % and a 12.8 % increase in the recorded COP. The simulation results consistently highlighted a 17.7 % and 9.84 % COP improvement at 3 and 4 kW, respectively. The evidence provided supports the development of more accurate simulations and paves the way for the practical implementation of genetic programming for actual product development.

CRediT authorship contribution statement

N. Giannetti: Writing – review & editing, Writing – original draft, Validation, Software, Methodology, Investigation, Formal analysis, Data curation, Conceptualization. **C.H. Kim:** Writing – review & editing, Writing – original draft, Investigation, Formal analysis, Data curation. **F. Della Santa:** Writing – review & editing, Writing – original draft, Investigation, Formal analysis, Conceptualization. **Y. Sei:** Writing – review & editing, Software, Methodology, Investigation, Formal analysis, Conceptualization. **K. Enoki:** Writing – review & editing, Validation, Supervision, Methodology, Investigation, Formal analysis, Data curation, Conceptualization. **K. Saito:** Writing – review & editing, Validation, Supervision, Resources, Project administration, Methodology, Investigation, Conceptualization.

Declaration of competing interest

The authors declare that they have no known competing financial interests or personal relationships that could have appeared to influence the work reported in this paper.

Acknowledgement

This study was based on the results obtained from the JPNP23001 project commissioned by the New Energy and Industrial Technology Development Organization (NEDO).

Appendix A. Supplementary data

Supplementary data to this article can be found online at https://doi.org/10.1016/j.applthermaleng.2025.129517.

Data availability

Data will be made available on request.

References

[1] A Computer Model for Air-Cooled Refrigerant Condenser with Specified Refrigerant Circuiting, ASHRAE Transactions, 1981.
[2] C.C. Wang, J.Y. Jang, C.C. Lai, Y.J. Chang, Effect of circuit arrangement on the performance of air-cooled condenser, Int. J. Refrig. 22 (4) (1999) 275–282.
[3] S.Y. Liang, T.N. Wong, G.K. Nathan, Study on refrigerant circuitry of condenser coils with exergy destruction analysis, Appl. Therm. Eng. 20 (6) (2000) 559–577.
[4] S.Y. Liang, T.N. Wong, G. Nathan, Numerical and experimental studies of refrigerant circuitry of evaporator coils, Int. J. Refrig. 24 (8) (2001) 823–833.
[5] L. Hu, T. Xiong, Y. Yang, G. Liu, G. Yan, Recent advances in refrigerant circuitry optimization of fin-and-tube heat exchangers for air source heat pump systems, Energy 333 (2025) 137443.
[6] D. Wang, C. Liu, D. Yu, J. Chen, Influence factors of flow distribution and a feeder tube compensation method in multi-circuit evaporators, Int. J. Refrig. 73 (2017) 11–23.
[7] J.-H. Kim, J.E. Braun, E.A. Groll, A hybrid method for refrigerant flow balancing in multi-circuit evaporators: upstream versus downstream flow control, Int. J. Refrig. 32 (6) (2009) 1271–1282.
[8] A.M. Bahman, E.A. Groll, Application of interleaved circuitry to improve evaporator effectiveness and COP of a packaged AC system, Int. J. Refrig. 79 (2017) 114–129.
[9] S. Ishaque, M.I.H. Siddiqui, M.H. Kim, Effect of heat exchanger design on seasonal performance of heat pump systems, Int. J. Heat Mass Transf. 151 (2020) 119404.
[10] Granryd, E. (1992). Optimum circuit tube length and pressure drop on the refrigerant side of evaporators. *International refrigeration and air conditioning conference*, paper 143.
[11] W.J. Lee, H.J. Kim, J.H. Jeong, Method for determining the optimum number of circuits for a fin–tube condenser in a heat pump, Int. J. Heat Mass Transf. 98 (2016) 462–471.
[12] Holland, J.H. (1975). *Adaptation in natural and artificial systems.* University of Michigan Press (2nd ed., MIT press, 1992).
[13] J. Larson, M. Menickelly, S.M. Wild, Derivative-free optimization methods, Acta Numerica 28 (2019) 287–404, https://doi.org/10.1017/S0962492919000060.
[14] X.S. Yang, Nature-inspired optimization algorithms: challenges and open problems, J. Comput. Sci. 46 (2020) 101104.
[15] M. Mitchell, An Introduction to Genetic Algorithms, MIT Press, 1998.
[16] The MathWorks, Inc. Global Optimization Toolbox User's Guide, (Chapter 9).
[17] J. McCall, Genetic algorithms for modelling and optimisation, J. Comput. Appl. Math. 184 (2005) 205–222.
[18] K. Deb, A. Pratap, S. Agarwal, T. Meyarivan, A fast and elitist multiobjective genetic algorithm: NSGA-II, IEEE Trans. Evol. Comput. 6 (2) (2002) 182–197.
[19] X.-S. Yang, Chapter 6 – Genetic algorithms, in: Nature-Inspired Optimization Algorithms, 2nd ed., Academic Press, 2021, pp. 91–100.
[20] S. Katoch, S.S. Chauhan, V. Kumar, A review on genetic algorithm: past, present, and future, Multimed. Tools Appl. 80 (2021) 8091–8126.
[21] L.G. Caldas, L.K. Norford, A design optimization tool based on a genetic algorithm, Autom. Constr. 11 (2) (2002) 173–184.
[22] W. Wang, R. Zmeureanu, H. Rivard, Applying multi-objective genetic algorithms in green building design optimization, Build. Environ. 40 (11) (2005) 1512–1525.
[23] K.P. Ferentinos, T.A. Tsiligiridis, Adaptive design optimization of wireless sensor networks using genetic algorithms, Comput. Netw. 51 (4) (2007) 1031–1051.
[24] F.S. Almeida, A.M. Awruch, Design optimization of composite laminated structures using genetic algorithms and finite element analysis, Compos. Struct. 88 (3) (2009) 443–454.
[25] F. Colombo, F. Della Santa, S. Pieraccini, Multi-objective optimisation of an aerostatic pad: design of position, number and diameter of the supply holes, J. Mech. (2019), https://doi.org/10.1017/jmech.2019.41.
[26] A. Braghin, L. Galuppi, G. Royer-Carfagni, Evaluation of a genetic algorithm for constrained multi-objective structural optimization in laminated glass design, Compos. Struct. 354 (2025) 118773.
[27] P.A. Domanski, Finned-Tube Evaporator Model with a Visual Interface, International Congress of Refrigeration, Sydney, Australia, 1999.
[28] P.A. Domanski, EVAP-COND Simulation Models for Finned Tube Heat Exchangers, National Institute of Standards and Technology, 2003.
[29] P.A. Domanski, Simulation of an Evaporator with Non-uniform One-Dimensional Air Distribution, ASHRAE Winter Meeting, New York, 1991.
[30] P.A. Domanski, D. Yashar, M. Kim, Performance of a finned-tube evaporator optimized for different refrigerants and its effects on system efficiency, Int. J. Refrig. 28 (6) (2005) 820–827.
[31] J.H. Lee, S.W. Bae, K.H. Bang, M.H. Kim, Experimental and numerical research on condenser performance for R-22 and R407-C refrigerants, Int. J. Refrig. 25 (3) (2002) 372–382.
[32] H. Jiang, V. Aute, R. Radermacher, CoilDesigner: a general-purpose simulation and design tool for air-to-refrigerant heat exchangers, Int. J. Refrig. 29 (2006) 601–610.
[33] J. Liu, W. Wei, G. Ding, C. Zhang, M. Fukaya, K. Wang, T. Inagaki, A general steady-state mathematical model for fin-and-tube heat exchanger based on graph theory, Int. J. Refrig. 27 (8) (2004) 965–973.

[34] Z. Li, B. Shen, K.R. Gluesenkamp, Multi-objective optimization of low-GWP mixture composition and heat exchanger circuitry configuration for improved system performance and reduced refrigerant flammability, Int. J. Refrig. 126 (2021) 133–142.
[35] J.C.S. Garcia, N. Giannetti, D.A.B. Varela, R.J. Varela, S. Yamaguchi, K. Saito, M. S. Berana, Design of a numerical simulator for finned-tube heat exchangers with arbitrary circuitry, Heat Transfer Eng. 43 (19) (2019).
[36] Z. Wu, G. Ding, K. Wang, M. Fukaya, Knowledge-based evolution method for optimizing refrigerant circuitry of fin-and-tube heat exchangers, HVAC&R Research 14 (3) (2008) 435–452.
[37] Z. Wu, G. Ding, K. Wang, M. Fukaya, Application of a genetic algorithm to optimize the refrigerant circuit of fin-and-tube heat exchangers, Int. J. Therm. Sci. 47 (8) (2008) 985–997.
[38] N. Ploskas, C. Laughman, A.U. Raghunathan, N.V. Sahinidis, Optimization of circuitry arrangements for heat exchangers using derivative-free optimization, Chem. Eng. Res. Des. 131 (2018) 16–28.
[39] Z. Li, V. Aute, J. Ling, Tube-fin heat exchanger circuitry optimization using integer permutation based genetic algorithm, Int. J. Refrig. 103 (2019) 135–144.
[40] S. Ishaque, M.H. Kim, Refrigerant circuitry optimization of finned tube heat exchangers using a dual-mode intelligent search algorithm, Appl. Therm. Eng. 212 (2022) 118576.
[41] N. Giannetti, J.C.S. Garcia, C.H. Kim, Y. Sei, K. Enoki, K. Saito, Circuitry optimization using genetic programming for the advancement of next generation refrigerants, Int. J. Heat Mass Transf. 217 (2023) 124648.
[42] Giannetti, N., Garcia, J.C.S., Varela, R.J., Sei, Y., Enoki, K., Jeong, J., Saito, K. (2021). Development of assessment techniques for next-generation refrigerants with low GWP values. Proceedings of the 2021 JSRAE annual conference, Tokyo.
[43] Z. Li, B. Shen, H. Wan, B. Fricke, Heat exchanger circuitry optimization using an enhanced integer permutation-based genetic algorithm in low-GWP reversible heat pump applications, Appl. Therm. Eng. 239 (2024) 122111.
[44] D. Ma, Q. Chen, G. Yan, Optimization study of the circuitry for 5 mm small-diameter finned-tube heat exchanger in air-source heat pumps, Appl. Therm. Eng. 248 (2024) 123359.
[45] N. Giannetti, A. Milazzo, J.C. Garcia, C.-H. Kim, Y. Sei, K. Enoki, K. Saito, Thermodynamic optimization of heat exchanger circuitry via genetic programming, Appl. Therm. Eng. 252 (2024) 123623.
[46] C.H. Kim, N. Giannetti, Y. Sei, K. Enoki, K. Saito, Simplification of evolutionarily optimized evaporator circuitry via key topological features. *Science and technology for the*, Built Environ. (2025), Manuscript ID STBE-0273-2025 (under review).
[47] Kim, C.H., Tanaka, C., Giannetti, N., Garcia, J.C.S., Sei, Y., Enoki, K., Saito, K. (2025). Evaporator circuitry optimization in a three-dimensional case. *35th international symposium on transport phenomena (ISTP)*.
[48] Li, Z., Ling, J., Aute, V. (2018). Tube-fin heat exchanger circuitry optimization using integer permutation based genetic algorithm. *International refrigeration and air conditioning conference*, paper 2035.
[49] R. Zhao, Z. Wang, Y. Sun, F. Wang, D. Huang, Effect of the number of circuits on a finned-tube heat exchanger performance and its improvement by a reversely variable circuitry, Appl. Sci. 12 (2022) 8960.
[50] D.A. Yashar, S. Lee, P.A. Domanski, Rooftop air-conditioning unit performance improvement using refrigerant circuitry optimization, Appl. Therm. Eng. 83 (2015) 81–87.
[51] J. Sim, H. Lee, J.H. Jeong, Optimal design of variable-path heat exchanger for energy efficiency improvement of air-source heat pump system, Appl. Energy 290 (2021).
[52] T. Xiong, H. Wu, L. Hu, G. Liu, G. Yan, Optimal design of vapor-bypassed heat exchanger for performance improvement of air source heat pump system, Renew. Energy 249 (2025) 123219.
[53] C.C. Wang, J.Y. Jang, N.F. Chiou, A heat transfer and friction correlation for wavy fin-and-tube heat exchangers, Int. J. Heat Mass Transf. 42 (1999) 1919–1924.
[54] F. Dittus, L. Boelter, Heat transfer in automobile radiators of the tubular type, Int. Commun. Heat Mass Transfer 12 (1) (1985) 3–22.
[55] M.M. Shah, Chart correlation for saturated boiling heat transfer: equations and further study, ASHRAE Trans. 88 (1) (1982) 185–196.
[56] H. Muller-Steinhagen, K. Heck, A simple friction pressure drop correlation for two-phase flow in pipes, Chem. Eng. Process. Process Intensif. 20 (6) (1986) 297–308.
[57] C. Popiel, J. Wojtkowiak, Friction factor in U-type undulated pipe flow, J. Fluids Eng. 122 (2) (2000) 260–263.
[58] P.A. Domanski, C. Hermes, An improved two-phase pressure drop correlation for 180° return bends, in: 3rd Asian Conference on Refrigeration and Air-Conditioning, Gyeongju, Korea, 2006.
[59] T. Pencheva, K. Atanassov, A. Shannon, Modelling of a roulette wheel selection operator in genetic algorithms using generalized nets, Bioautomation 13 (2009) 257–264.
[60] N. Giannetti, S. Matsui, R. Mori, J. Jeong, H. Ariyadi, Y. Miyaoka, E. Togashi, K. Saito, Emulator-type load-based tests for dynamic performance characterization of air conditioners, Energ. Buildings 273 (2022) 112411.
[61] JIS B 8631, *Performance, test conditions and methods for refrigerated display cabinets* (in Japanese), 2011.